Impact of lattice strain on the tunnel magnetoresistance in Fe/insulator/Fe and Fe/insulator/La$_{0.67}$Sr$_{0.33}$MnO$_3$ magnetic tunnel junctions

A. Useinov,[1,*] Y. Saeed,[2] N. Singh,[2] N. Useinov,[3] and U. Schwingenschlögl[2,†]

[1]*Department of Physics, California State University, Northridge, California 91330, USA*
[2]*PSE Division, King Abdullah University of Science and Technology, Thuwal 23955, Saudi Arabia*
[3]*Department of Solid State Physics, Kazan Federal University, Kazan, Russia*

The objective of this work is to describe the tunnel electron current in single-barrier magnetic tunnel junctions within an approach that goes beyond the single-band transport model. We propose a ballistic multichannel electron transport model that can explain the influence of in-plane lattice strain on the tunnel magnetoresistance as well as the asymmetric voltage behavior. We consider as an example single-crystal magnetic Fe(110) electrodes for Fe/insulator/Fe and Fe/insulator/La$_{0.67}$Sr$_{0.33}$MnO$_3$ tunnel junctions, where the electronic band structures of Fe and La$_{0.67}$Sr$_{0.33}$MnO$_3$ are derived by *ab initio* calculations.

I. INTRODUCTION

One of the fast-growing directions in modern magnetic electronics (spintronics) is the field of magnetic tunnel junctions (MTJs) and their applications, for example, as basic elements in magnetic random access memories, read heads of hard drives, and magnetic field sensors. The potential to realize memristors and vortex oscillators creates additional incentive for future investments in this area.[1,2] MTJs such as FM/insulator/FM and FM/insulator/HM heterostructures, where FM is a ferromagnet (such as Co, Fe, CoFeB), the insulator is ferroelectric (such as BaTiO$_3$, PbTiO$_3$), and HM is a half metal (such as La$_{0.67}$Sr$_{0.33}$MnO$_3$, Co$_2$MnSn), are very promising, because they combine magnetic, ferroelectric, and spin filtering properties. Tunnel electroresistance and tunnel magnetoresistance (TMR) effects may coexist in these systems. The TMR arises from states of different resistance for parallel and antiparallel magnetic alignments, while the tunnel electroresistance relies on the polarization of the ferroelectric insulator. The insulating layer has to be thick enough to yield strong ferroelectricity, which usually rapidly disappears for decreasing thickness, and has to be thin enough for electron tunneling. Moreover, the ferroelectric polarization in thin ferroelectric films is conjugated with the magnitude of the lattice strain.[3–6] A high ferroelectric polarization is achieved by epitaxial film growth with an initially high difference between the in-plane lattice parameters of the substrate and the deposited layers. Obviously, the electronic band structures and transport properties of the strained FM and HM layers can be fundamentally different from those without strain.

The objective of this work is to establish the interplay between the lattice strain and the magnitude of the TMR using a multiband approach for the electron transport. We predict that for strained symmetric MTJs the TMR is reduced, because of changes in the electronic band structure under strain. In general, the tunnel electroresistance in ferroelectric TJs should logarithmically increase with the ferroelectric polarization (assuming that the in-plane strain increases), as was shown, for instance, in the theoretical works of Zhuravlev and coworkers.[7,8] This means there is a balanced configuration of the insulator thickness (potential barrier thickness) and strain that provides the highest TMR and tunnel electroresistance. To calculate the tunnel current and TMR we have to go beyond the assumption of two conduction channels (single-band model) similar to Refs. 9–15.

Investigation of MTJs has a long history.[16–19] In Ref. 16 Valet and Fert have introduced basic principles for the qualitative and quantitative interpretation of the spin-polarized electron transport in magnetic multilayer structures, based on Boltzmann-like equations. An alternative theoretical approach of electronic transport through nanocontacts with and without domain walls between two FM electrodes has been developed in Ref. 20. This theory utilizes quasiclassical as well as quantum mechanical ideas and is based on extended Boltzmann-like equations. Boundary conditions on the interfaces of the junction are taken into account as a key part of the solution. The theory can be adapted to the case of ballistic transport through single-barrier[14] and double-barrier[21] planar junctions.

Using the universality of the above technique, we formulate a multichannel (or multiband) approach following the ideas of Ref. 22. The tunneling conductance in MTJs can be written in terms of the averaged spin-dependent tunneling probabilities of the conduction channels for parallel (P) and antiparallel (AP) magnetizations. According to our *ab initio* calculations for Fe, several minority and majority spin bands cross the Fermi level, representing different electron wave functions. We extract the dispersion relations along the tunneling direction [perpendicular to the Fe(110) interface] from the bulk band structure. For simplicity, the insulator is considered to be homogeneous. Our approach does not incorporate filtering effects inside the barrier, which are important in the case of MgO or for the splitting of the valence band in SrTiO$_3$ and BaTiO$_3$, for instance.[18,23,24]

II. THE MULTICHANNEL APPROACH

The ideas of the multichannel approach are demonstrated in Fig. 1. In this model each propagating channel is associated with a given spin and symmetry of the wave function. The emitter provides electrons with different Fermi vectors, which tunnel across the barrier into the states of the collector. We employ a formula for the current density originally derived for transport through a magnetic planar junction.[14] For the
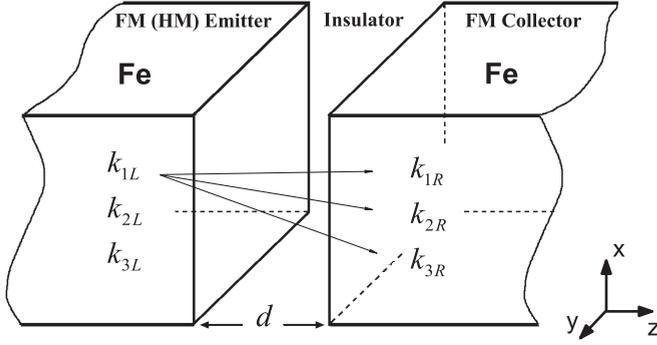
FIG. 1. Simplified schema of the multichannel model of a single-crystal MTJ for positive bias (electrons tunnel from left to right). The model assumes independent propagation channels, each being associated with a given spin and symmetry.

single-band model the current density is proportional to the integral of the product of the transmission coefficient, $D^{P(AP)}$, and the cosine of the incidence angle of the electron trajectory, $\cos(\theta_L^{\uparrow,\downarrow})$. The angle $\theta_L^{\uparrow,\downarrow}$ is measured from the normal (transport direction) to the interface plane (L: left, R: right). The integral is taken over $d\Omega_L = \sin(\theta_L)d\theta_L d\phi$:

$$J_{\uparrow,\downarrow}^{P(AP)} = \frac{e^2 V (k_L^{\uparrow,\downarrow})^2}{4\pi^2 \hbar} \langle \cos(\theta_L^{\uparrow,\downarrow}) D_{\uparrow,\downarrow}^{P(AP)} \rangle_{\Omega_L}. \qquad (1)$$

Here $k_L^{\uparrow,\downarrow}$ is the absolute value of the Fermi vector of the left-hand electrode and $\uparrow,\downarrow$ is the spin index. The transmission coefficient is a function of the applied voltage V, of $\theta_L^{\uparrow,\downarrow} = 0... \arccos(\sqrt{|1 - (k_R^{\uparrow,\downarrow}/k_L^{\uparrow,\downarrow})^2|})$, and of $k_{L(R)}^{\uparrow,\downarrow}$. With $x^{\uparrow,\downarrow} = \cos(\theta_L^{\uparrow,\downarrow})$ we can write

$$\langle x^{\uparrow,\downarrow} D_{\uparrow,\downarrow}^{P(AP)} \rangle_{\Omega_L} = \int_{X^{\uparrow,\downarrow}}^{1} x^{\uparrow,\downarrow} D_{\uparrow,\downarrow}^{P(AP)} dx^{\uparrow,\downarrow},$$

where the lower limit $X^{\uparrow,\downarrow}$ for the integration arises from the conservation of the projection of the Fermi vector in the xy plane: $k_{\parallel}^{\uparrow,\downarrow} = k_L^{\uparrow,\downarrow} \sin(\theta_L^{\uparrow,\downarrow}) = k_R^{\uparrow,\downarrow} \sin(\theta_R^{\uparrow,\downarrow})$. It equals zero when the electrons tunnel from the left minority into the right majority conduction band and $X^{\uparrow,\downarrow} = \sqrt{|1 - (k_R^{\uparrow,\downarrow}/k_L^{\uparrow,\downarrow})^2|}$ when they tunnel from the left majority into the right minority conduction band. For the multiband approach the majority and minority bands can be both spin-up and spin-down for any magnetic configuration.

To achieve a multichannel model (or model with multiband tunnel relations) for single-crystal junctions we redefine the current density in Eq. (1):

$$J_{\uparrow,\downarrow}^{P(AP)} = \frac{e^2 V}{4\pi^2 \hbar} \sum_{\eta=1}^{N} \sum_{\mu=1}^{M} (k_\eta^{\uparrow,\downarrow})^2$$
$$\times \langle \cos(\theta_\eta) D_{\eta,\mu}^{P(AP)}(k_\eta^{\uparrow,\downarrow}, k_\mu^{\uparrow,\downarrow(\downarrow,\uparrow)}) \rangle_{\Omega_L}. \qquad (2)$$

Here η and μ are the indices of the left-hand and right-hand bands, respectively, and N and M are the numbers of bands. The combinations $\{\eta,\mu\}$, see Fig. 1, identify the conduction relations between the bands through the barrier. Equation (2) is valid for positive bias. The solution for negative bias is derived using symmetric relations of the system; i.e., the collector and

emitter are exchanged ($k_\eta \to k_\mu$, $k_\mu \to k_\eta$). We assume that there is no spin-flip leakage and that a conduction channel is available between any left-hand and right-hand bands with the same spin. Otherwise the electrons are reflected back, giving rise to a resistance. Note that the lowest conductance corresponds to the largest difference in the density of states at the Fermi level between the left and right electrodes. Regarding the transmission coefficient for the single-barrier system, the basic mathematical expressions can be found in Ref. 14, where an exact quantum mechanical solution has been derived employing Airy functions for the tunnel barrier.

Since we obtain the band structures by *ab initio* calculations based on density functional theory, the effects of orbital hybridizations are modeled fully realistically. The resulting band structures for bulk Fe (space goup *Cmmm*) and $La_{0.67}Sr_{0.33}MnO_3$ are shown in Figs. 2 and 3, as derived using the WIEN2K package.[25] The exchange-correlation potential is parametrized in the generalized gradient approximation.[26] For the wave function expansion inside the atomic spheres a maximum value of the angular momentum of $\ell_{max} = 12$ is employed and a plane-wave cutoff of $R_{mt} K_{max} = 9$ with $G_{max} = 24$ is used. Self-consistency is assumed when the total energy variation reaches less than 10^{-4} Ry. We use a mesh of $10 \times 10 \times 10$ k points for calculating the electronic structure in order to describe the ground states of the compounds with high accuracy.
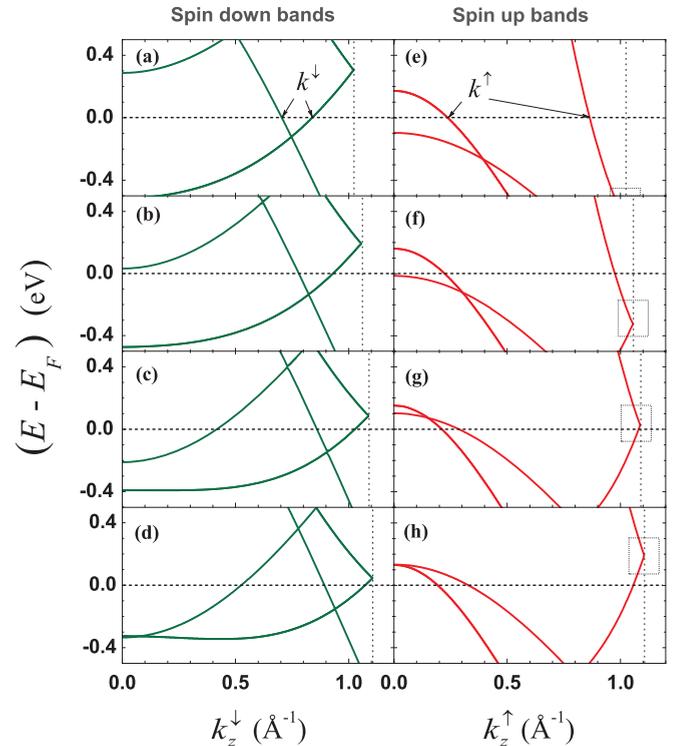

FIG. 2. (Color online) Electronic bands for bulk Fe along the Γ-Z direction. $E - E_F = 0$ corresponds to zero bias. Data are derived for different lattice parameters, which correspond to different lattice strains. The four band structures refer to (a), (e) $a = 3.875$ Å, $c = 3.083$ Å; (b), (f) $a = 3.937$ Å, $c = 2.986$ Å; (c), (g) $a = 3.999$ Å, $c = 2.894$ Å; (d), (h) $a = 4.030$ Å, $c = 2.850$ Å. The Γ point is located at $k_z^{\uparrow,\downarrow} = 0$ and the Z point is shown by vertical dotted lines.
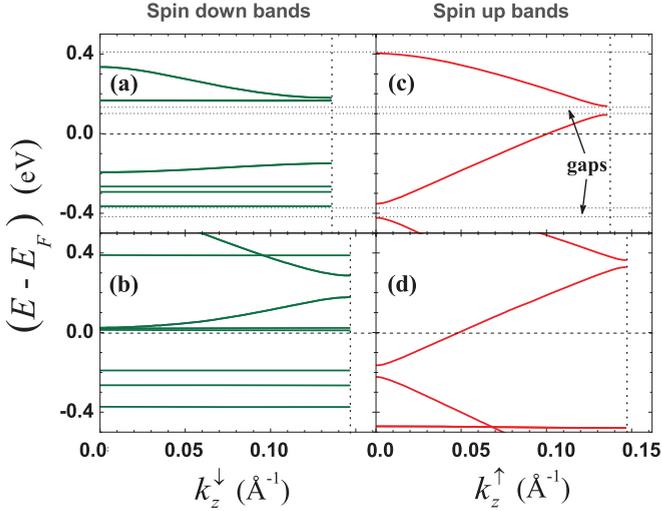
FIG. 3. (Color online) Electronic bands for bulk La$_{0.67}$Sr$_{0.33}$MnO$_3$ along the Γ-Z direction. $E - E_F = 0$ corresponds to zero bias. Data are derived for different lattice parameters, which correspond to different lattice strains. The two band structures refer to (a), (c) $a = 3.875$ Å, $c = 23.250$ Å and (b), (d) $a = 4.030$ Å, $c = 21.496$ Å. The Γ point is located at $k_z^{\uparrow,\downarrow} = 0$ and the Z point is shown by vertical dotted lines.

Figure 2 shows the band structure of Fe for different in-plane lattice parameters $a = 3.875$ Å, 3.937 Å, 3.999 Å, and 4.030 Å (bulk value), where red and green colors represent the two spins. As an example, we consider the symmetric Fe/insulator/Fe junction and demonstrate how to collect the conducting spin channels via the applied bias V. The bands of the left electrode (emitter) are the same as those of the right electrode (collector) and the Fermi energies $E_F^L = E_F^R = E_F$ are equal at zero bias. Horizontal dashed lines represent E_F, which intersects with the bands at the Fermi vectors $k_{\eta(\mu)}^{\uparrow,\downarrow}$. In particular, in Figs. 2(a), 2(b) and Figs. 2(e), 2(f) the system has two $k^{\downarrow}$ and two $k^{\uparrow}$ vectors at zero bias, while in the case of Figs. 2(c), 2(d), 2(g), 2(h) E_F is intersected by three spin-up and three spin-down bands. We thus have the Fermi vector set $\{k_{1L(R)}^{\uparrow,\downarrow}, k_{2L(R)}^{\uparrow,\downarrow}, k_{3L(R)}^{\uparrow,\downarrow}\}$. In the case of positive (negative) bias, by definition, E_F of the left electrode shifts up (down) in energy, while for the right electrode it shifts down (up) by the same amount. The voltage drop is $|E_F^L - E_F^R| = |eV|$. As a result the Fermi vector set is changed. As an example, let us set $V = +0.8$ V with $E_F^L = 0.4$ eV and $E_F^R = -0.4$ eV. According to Figs. 2(a) and 2(e), for the left electrode this results in the Fermi vector sets $\{0, 0, k_{3L}^{\uparrow}\}$ and $\{k_{1L}^{\downarrow}, k_{2L}^{\downarrow}, k_{3L}^{\downarrow}\}$ and for the right electrode in the sets $\{k_{1R}^{\uparrow}, k_{2R}^{\uparrow}, k_{3R}^{\uparrow}\}$ and $\{0, k_{2R}^{\downarrow}, k_{3R}^{\downarrow}\}$, which generates $1 \times 3 = 3$ channels for spin-up and $3 \times 2 = 6$ channels for spin-down, for the parallel magnetization. In contrast, $1 \times 2 = 2$ channels for spin-up and $3 \times 3 = 9$ channels for spin-down are generated in the case of the antiparallel magnetization. Thus, the current can be represented by $3 \times 3 = 9$ channels for each spin orientation (in the general case: $N \times M$). When the Fermi vectors vanish we have, of course, a nonconducting channel with vanishing current density.

Figure 3 shows the band structure of La$_{0.67}$Sr$_{0.33}$MnO$_3$ along the Γ-Z direction for two sets of lattice parameters: $a = 3.875$ Å, $c = 23.250$ Å and $a = 4.030$ Å, $c = 21.496$ Å.

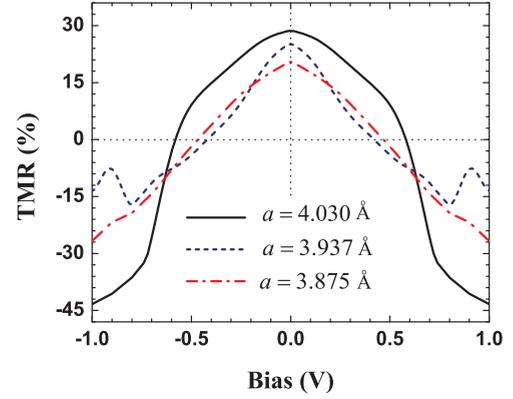FIG. 4. (Color online) TMR versus applied voltage for Fe/insulator/Fe MTJs with the lattice parameters $a = 3.875$ Å, 3.937 Å, and 4.030 Å. The barrier parameters are $d = 1.8$ nm and $U_B = 2.8$ eV.

The Fermi vector, transmission coefficient, and current density for each band are derived as demonstrated before. However, some of the spin-down bands are very flat with energy gaps between them, in contrast to the spin-up bands. As a function of the bias the system therefore switches between a HM and FM. However, there are also energies at which neither spin-up nor spin-down states exist.

III. TUNNEL MAGNETORESISTANCE UNDER STRAIN

Physical parameters that characterize the properties of MTJs are the total tunnel current density $J^{\mathrm{P(AP)}} = (J_{\uparrow} + J_{\downarrow})^{\mathrm{P(AP)}}$, the TMR $= (J^{\mathrm{P}} - J^{\mathrm{AP}})/J^{\mathrm{AP}} \times 100\%$, the normalized TMR$_{\mathrm{n}} = (J^{\mathrm{P}} - J^{\mathrm{AP}})/J^{\mathrm{AP}} \times$ TMR$^{-1}(V = 0)$, and the output voltage $V_{\mathrm{out}} = V(J^{\mathrm{P}} - J^{\mathrm{AP}})/J^{\mathrm{AP}}$, which can be obtained from free-electron[12,27] or tight-binding[13,15] models. However, unfortunately these models do not reproduce the experimental effect of strain on the charge transport characteristics. A single-band approach is sufficient to model the TMR in amorphous sputtered MTJs[28] and can satisfactorily describe the TMR$_{\mathrm{n}}$ and V_{out} of epitaxial single- and double-barrier FeCoB/MgO junctions.[29] In our case we have to go beyond parabolic dispersions and the single-band
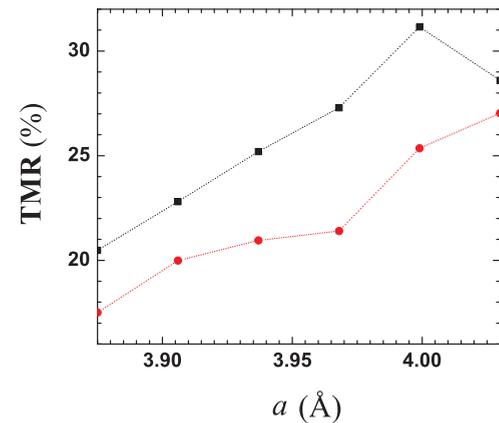

FIG. 5. (Color online) TMR as function of the lattice parameter a for Fe/insulator/Fe MTJs. Black and red colors refer to biases of 0.1 mV and 0.1 V, respectively.
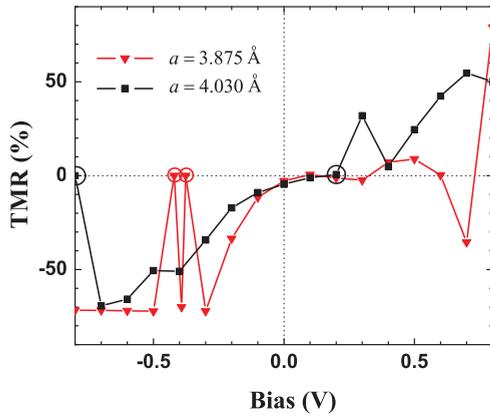
FIG. 6. (Color online) TMR versus applied bias for the Fe/insulator/La$_{0.67}$Sr$_{0.33}$MnO$_3$ MTJ. The barrier parameters are $d = 1.8$ nm, $U_B = 2.8$ eV, and $m_B = 0.25$.

model, however, keeping the simplicity of the approach. For the Fermi vectors derived above as well as for typical parameters of an Al$_2$O$_3$ tunnel barrier, TMR results derived by Eq. (2) are shown in Figs. 4, 5, and 6. The barrier thickness is set to $d = 1.8$ nm, the barrier height above E_F to $U_B = 2.8$ eV, and the effective mass to $m_B = 0.25$.[30] In our calculations for metals the effective mass is equal to the free-electron mass.

Figure 4 presents the TMR as function of the bias for different lattice parameters, showing that the TMR, in general, behaves nonmonotonically. For unstrained Fe ($a = 4.030$ Å) a decreasing in-plane lattice parameter (increasing strain) leads to a lower TMR. Figure 5 gives the TMR as a function of the lattice parameter for zero and 0.1 V bias. Interestingly, we observe deviations from a linear behavior: For almost zero bias the TMR increases up to 31.1% for $a = 3.999$ Å, 28.6% for $a = 4.030$ Å, and 27.3% for $a = 3.968$ Å. This behavior is related to modifications in the reflection of the majority states at the Z point, where the Fermi vector achieves its maximal magnitude (Fig. 2, dashed rectangles). Note that these states give the main contribution to the tunnel current. The observed differences for different in-plane lattice parameters are explained by variations of the band structure. The dashed rectangles in Figs. 2(e)–2(h) demonstrate the bands near the Z point. For $a = 3.999$ Å, see Fig. 2(g), the majority band intersects the Fermi level at the Z point, favoring J^P over J^{AP}, in contrast to the other lattice parameters. The maximal TMR value close to zero bias is in good agreement with the results of Yuasa and coworkers for Fe(110)/Al$_2$O$_3$/Fe$_{50}$Co$_{50}$, see Fig. 3(b) in Ref. 30, and of Hauch and coworkers for Fe(110)/MgO(111)/Fe(110), 28% at $T = 300$ K.[31]

In the case of the Fe/insulator/La$_{0.67}$Sr$_{0.33}$MnO$_3$ MTJ our model gives a positive TMR for $V > 0.11$ V as well as a negative TMR below; see Fig. 6. The TMR curves are qualitatively similar to those obtained experimentally

for Co/SrTiO$_3$/La$_{0.7}$Sr$_{0.3}$MnO$_3$[32] and agree with the room temperature TMR in Fe/MgO/Co$_2$MnSn (about -5% at a bias of 0.1 mV[33]). However, according to these authors the TMR is suppressed in the voltage range $|V| \geqslant 0.5$ V, which is probably related to enhanced spin scattering for high bias. TMR curves are given in Fig. 6 for the in-plane lattice parameters $a = 4.030$ Å and $a = 3.875$ Å, where the latter corresponds to unstrained La$_{0.67}$Sr$_{0.33}$MnO$_3$. For positive bias the magnitude of the TMR decreases with the Fe lattice strain, whereas for negative bias the situation is reversed. For the circled points in Fig. 6, where the TMR goes to zero, both spin channels are closed, compare the energy gaps in Fig. 3, because of $J^P = J^{AP} = 0$. There are other points where the TMR is zero as $J^P = J^{AP}$. Variation of the effective mass in the tunnel barrier leads to a weak response of the TMR in symmetric (1.5% decrease) and a strong response in asymmetric (14% increase) junctions, for all lattice parameters close to zero bias, $m_B = 1$.

IV. CONCLUSION

We have extended an established quasiclassical ballistic transport model to multichannel conductance, which has enabled us to investigate the role of the electronic band structure and the effect of strain on the transport properties of single-crystal Fe/insulator/Fe and Fe/insulator/La$_{0.67}$Sr$_{0.33}$MnO$_3$ MTJs. Our approach takes into account all bands of the FM and HM along the Γ-Z direction (direction of tunneling). We have demonstrated for typical parameters of an Al$_2$O$_3$ tunnel barrier a maximal TMR of 31.1% for the Fe/insulator/Fe MTJ, which is in good agreement with the experiment. A negative TMR of 5% is found for the Fe/insulator/La$_{0.67}$Sr$_{0.33}$MnO$_3$ MTJ close to zero bias, where the dependence on the bias reproduces experimental findings. The developed technique thus has demonstrated great potential for further studies on transport properties (including the spin transfer torque) in simple and magnetic TJs.

Strain effects on the TMR have been explored theoretically with a multiband approach. For the Fe/insulator/Fe MTJ it turns out that for small bias the TMR decreases linearly with the in-plane strain at the interface, whereas in the case of the Fe/insulator/La$_{0.67}$Sr$_{0.33}$MnO$_3$ MTJ the strain effects strongly depend on the sign of the applied bias. For positive bias it is positive and maximal for unstrained Fe, while for negative bias it is negative and the amplitude increases with strain and bias. The observed relations between the strain and the TMR are explained by variations of the band structure. We have demonstrated that in-plane strain can increase and decrease the TMR and therefore makes it possible to obtain optimal regimes for MTJ applications.

*artur.useinov@csun.edu

†udo.schwingenschlogl@kaust.edu.sa

[1] A. Dussaux, B. Georges, J. Grollier, V. Cros, A. V. Khvalkovskiy, A. Fukushima, M. Konoto, H. Kubota, K. Yakushiji, S. Yuasa, K. A. Zvezdin, K. Ando, and A. Fert, Nat. Commun. **1**, 10 (2010).

[2] A. Chanthbouala, R. Matsumoto, J. Grollier, V. Cros, A. Anane, A. Fert, A. V. Khvalkovskiy, K. A. Zvezdin, K. Nishimura, Y. Nagamine, H. Maehara, K. Tsunekawa, A. Fukushima, and S. Yuasa, Nat. Phys. **7**, 626 (2011).

[3] N. A. Pertsev, A. G. Zembilgotov, and A. K. Tagantsev, Phys. Rev. Lett. **80**, 1988 (1998).

[4] Y. S. Kim, D. H. Kim, J. D. Kim, and Y. J. Chang, Appl. Phys. Lett. **86**, 102907 (2005).

[5] H. Kohlstedt, N. A. Pertsev, J. Rodriguez Contreras, and R. Waser, Phys. Rev. B **72**, 125341 (2005).

[6] A. Petraru, N. A. Pertsev, and H. Kohlstedt, J. Appl. Phys. **101**, 114106 (2007).

[7] M. Y. Zhuravlev, R. F. Sabirianov, S. S. Jaswal, and E. Y. Tsymbal, Phys. Rev. Lett. **94**, 246802 (2005).

[8] M. Ye. Zhuravlev, S. Maekawa, and E. Y. Tsymbal, Phys. Rev. B **81**, 104419 (2010).

[9] N. Mott, Proc. R. Soc. London **153**, 699 (1936).

[10] I. Campbell, A. Fert, and A. Pomeroy, Philos. Mag. **15**, 977 (1967).

[11] M. Julliere, Phys. Lett. A **54**, 225 (1975).

[12] A. Manchon, N. Ryzhanova, N. Strelkov, A. Vedyayev, and B. Dieny, J. Phys.: Condens. Matter **19**, 165212 (2007).

[13] A. Kalitsov, M. Chshiev, I. Theodonis, N. Kioussis, and W. H. Butler, Phys. Rev. B **79**, 174416 (2009).

[14] A. Useinov, R. Deminov, N. Useinov, and L. Tagirov, Phys. Status Solidi B **247**, 1797 (2010).

[15] Y.-H. Tang, N. Kioussis, A. Kalitsov, W. H. Butler, and R. Car, Phys. Rev. B **81**, 054437 (2010).

[16] T. Valet and A. Fert, Phys. Rev. B **48**, 7099 (1993).

[17] P. Seneor, A. Fert, J.-L. Maurice, F. Montaigne, F. Petro, and A. Vaures, Appl. Phys. Lett. **74**, 4017 (1999).

[18] W. H. Butler, X.-G. Zhang, T. C. Schulthess, and J. M. MacLaren, Phys. Rev. B **63**, 054416 (2001).

[19] J. Mathon and A. Umerski, Phys. Rev. B **63**, 220403 (2001).

[20] A. Useinov, R. Deminov, L. Tagirov, and G. Pan, J. Phys.: Condens. Matter **19**, 196215 (2007).

[21] A. N. Useinov, J. Kosel, N. K. Useinov, and L. R. Tagirov, Phys. Rev. B **84**, 085424 (2011).

[22] C. Tiusan, F. Greullet, and M. Hehn, J. Phys.: Condens. Matter **19**, 165201 (2007).

[23] E. Tsymbal, K. Belashchenko, J. Velev, and S. Jaswal, Prog. Mater. Sci. **52**, 401 (2007).

[24] J. Velev, C. G. Duan, J. Burton, A. Smogunov, M. Niranjan, E. Tosatti, S. Jaswal, and E. Tsymbal, Nano Lett. **9**, 427 (2009).

[25] P. Blaha, K. Schwarz, G. Madsen, D. Kvasicka, and J. Luitz, *WIEN2k, An Augmented Plane Wave Plus Local Orbitals Program for Calculating Crystal Properties* (TU Vienna, Vienna, 2001).

[26] J. P. Perdew, K. Burke, and M. Ernzerhof, Phys. Rev. Lett. **77**, 3865 (1996).

[27] A. Useinov, O. Mryasov, and J. Kosel, J. Magn. Magn. Mater. **324**, 2844 (2012).

[28] D. Djayaprawira, K. Tsunekawa, M. Nagai, H. Maehara, S. Yamagata, N. Watanabe, S. Yuasa, Y. Suzuki, and K. Ando, Appl. Phys. Lett. **86**, 092502 (2005).

[29] G. Feng, S. Dijken, J. Feng, J. Coey, T. Leo, and D. Smith, J. Appl. Phys. **105**, 033916 (2009).

[30] S. Yuasa, T. Sato, E. Tamura, Y. Suzuki, H. Yamamori, K. Ando, and T. Katayama, Europhys. Lett. **52**, 344 (2000).

[31] J. O. Hauch, M. Fonin, M. Fraune, P. Turban, R. Guerrero, F. G. Aliev, J. Mayer, U. Rüdiger, and G. Güntherodt, Appl. Phys. Lett. **93**, 083512 (2008).

[32] J. M. De Teresa, A. Barthelemy, A. Fert, J. P. Contour, R. Lyonnet, F. Montaigne, P. Seneor, and A. Vaures, Phys. Rev. Lett. **82**, 4288 (1999).

[33] M. A. Tanaka, T. Hori, K. Kondou, T. Ono, S. Kasai, T. Asaka, and J. Inoue, J. Appl. Phys. **110**, 073905 (2011).